








# Noncoding SNP at rs1663689 represses ADGRG6 via interchromosomal interaction and reduces lung cancer progression

Xinyue Lei<sup>1,†</sup> , Xiaoling Tian<sup>1,†</sup> , Hao Wang<sup>1</sup> , Xinran Xu<sup>2</sup>, Guoli Li<sup>1</sup> , Wenxu Liu<sup>1</sup>, Dan Wang<sup>1</sup> , Zengtuan Xiao<sup>1</sup>, Mengzhe Zhang<sup>1</sup>, Mulin Jun Li<sup>2</sup> , Zhenfa Zhang<sup>1</sup>, Zhenyi Ma<sup>3</sup> & Zhe Liu<sup>1,2,3,4,\*</sup> 

## Abstract

A previous genome-wide association study (GWAS) revealed an association of the noncoding SNP rs1663689 with susceptibility to lung cancer in the Chinese population. However, the underlying mechanism is unknown. In this study, using allele-specific 4C-seq in heterozygous lung cancer cells combined with epigenetic information from CRISPR/Cas9-edited cell lines, we show that the rs1663689 C/C variant represses the expression of ADGRG6, a gene located on a separate chromosome, through an interchromosomal interaction of the rs1663689 bearing region with the ADGRG6 promoter. This reduces downstream cAMP-PKA signaling and subsequently tumor growth both *in vitro* and in xenograft models. Using patient-derived organoids, we show that rs1663689 T/T—but not C/C—bearing lung tumors are sensitive to the PKA inhibitor H89, potentially informing therapeutic strategies. Our study identifies a genetic variant-mediated interchromosomal interaction underlying ADGRG6 regulation and suggests that targeting the cAMP-PKA signaling pathway may be beneficial in lung cancer patients bearing the homozygous risk genotype at rs1663689.

**Keywords** ADGRG6; cAMP-PKA; interchromosomal interaction; lung cancer outcome; noncoding SNP

**Subject Categories** Cancer; Chromatin, Transcription & Genomics

**DOI** 10.15252/embr.202256212 | Received 30 September 2022 | Revised 5 April 2023 | Accepted 18 April 2023 | Published online 8 May 2023

**EMBO Reports (2023) 24: e56212**

## Introduction

Lung cancer is one of the most frequently diagnosed cancers and the leading cause of cancer mortality worldwide, with an estimated 5-

year survival rate of approximately 19% (Paz-Ares *et al*, 2008; Gadgeel *et al*, 2011; Ferlay *et al*, 2015; Bray *et al*, 2018; Bade & Dela Cruz, 2020). Small-cell lung carcinoma (SCLC) and non-small-cell lung carcinoma (NSCLC) are two major histological subtypes, accounting for 15 and 85% of all lung cancers, respectively. NSCLC consists primarily of adenocarcinoma (LUAD), squamous cell carcinoma (LUSC), and large cell carcinoma (LCC; Zappa & Mousa, 2016; Siegel *et al*, 2017). For patients with early-stage lung cancer, surgery is generally recommended, while patients with advanced lung cancer generally benefit from molecular targeted therapy (Vansteenkiste *et al*, 2014) and platinum-based doublet therapy (Bradley *et al*, 2015; Senan *et al*, 2016). Recent studies have revealed extensive genetic diversity both between and within tumors. This heterogeneity affects phenotypic variation and differential responses to therapeutic drugs. Understanding molecular heterogeneity is critical for precision medicine to tailor cancer treatments to the specific features of a patient's disease. For example, lung adenocarcinoma comprises genetic subtypes with distinct, mutually exclusive alterations in genes such as *EGFR*, *KRAS*, or *ALK*, and targeting *EGFR*- or *ALK*-mutant tumors with targeted inhibitors prolongs survival and improves the patient outcome (Collisson & Howell, 2014; Lin *et al*, 2016; Remon *et al*, 2019a, 2019b, 2019c).

In addition to these well-known tumor-specific somatic mutations, germline mutations also make great contributions to interpatient heterogeneity. Genome-wide association studies (GWAS) previously identified 81 lung cancer susceptibility variants in 51 loci that are robustly associated with lung cancer risk (Bosse & Amos, 2018; Dai *et al*, 2019). Functional analysis of these SNPs will improve our understanding of lung tumor etiology and the development of personalized treatment. However, as the vast majority (> 80%) of GWAS hits are located in noncoding regions of the genome, often at considerable genomic distances from annotated genes, making an assessment of their potential function in disease

1 Department of Lung Cancer Center, Tianjin Medical University Cancer Institute and Hospital, Haihe Laboratory of Cell Ecosystem, State Key Laboratory of Experimental Hematology, Department of Urology, The Second Hospital of Tianjin Medical University, Key Laboratory of Immune Microenvironment and Disease of the Ministry of Education, Department of Immunology, School of Basic Medical Sciences, Tianjin Medical University, Tianjin, China

2 Department of Pharmacology, School of Basic Medical Sciences, Tianjin Medical University, Tianjin, China

3 Key Laboratory of Aging and Cancer Biology of Zhejiang Province, Department of Cell Biology, School of Basic Medical Sciences, Hangzhou Normal University, Hangzhou, China

4 Collaborative Innovation Center for Cancer Personalized Medicine, Nanjing Medical University, Nanjing, China

\*Corresponding author. Tel. +86-22-83336533; Fax. +86-22-83336533; E-mail: zheliu@tmu.edu.cn

†These authors contributed equally to this work as first authors

etiology problematic (Hindorf *et al*, 2009; Freedman *et al*, 2011; Javierre *et al*, 2016). The majority of cancer-associated noncoding genetic variants are functionally uncharacterized.

It has been reported in a GWAS of a Chinese population that SNP locus rs1663689 is associated with lung cancer susceptibility and that the variant C allele is the protective allele (Dong *et al*, 2012). The distribution of the C allele show racial disparity, with a frequency (ALFA) of 20.431% in the European and 50% in the Asian population. rs1663689 is located within an intergenic region at chromosome 10p14. Its upstream neighboring gene is *GATA3*, and its downstream neighboring gene is *CELF2*. In this study, we observed a risk-preventive association between the rs1663689 variant with lung cancer outcome. Using allele-specific 4C-seq in combination with genome-wide epigenetic information, we found that rather than regulating its neighboring genes, rs1663689 regulates the expression of *ADGRG6*, a gene located on chromosome 6, via interchromosomal interaction and subsequently modulates the cAMP-PKA pathway. Further, we showed that the PKA inhibitor H89 exhibits a striking inhibitory effect on patient-derived lung cancer organoids carrying the T/T genotype at rs1663689. Our studies demonstrated a nontraditional trans-effect of a genetic variant and suggest a novel personalized treatment strategy for lung cancer patients harboring the T/T genotype at rs1663689.

## Results and Discussion

### The rs1663689 variant reduces proliferation and invasion *in vitro*

To explore the mechanism by which rs1663689 regulates lung cancer, we generated isogenic lung cancer cell lines homozygous for the minor (C/C) allele from the major allele (T/T)-bearing lung cancer line H460 with the CRISPR/Cas9 technique. To exclude potential off-target effects, we also generated T/T and C/C lines from a different human lung cancer line, A549, which has the T/C genotype. Parental H460 (T/T) and A549 (T/C) cells were also exposed to the CRISPR/Cas9 complex. We confirmed the successful targeting of rs1663689 by Sanger sequencing (Fig 1A) and then tested the resultant differences in cellular behavior function. In a two-dimensional culture of H460 and A549 lines, the C allele of rs1663689 was associated with reduced proliferation but enhanced cell death in both lines, as evaluated by 5-bromodeoxyuridine (BrdU) and Cell Death ELISA assays (Fig 1B and C). Consistently, a significantly higher level of cleaved Caspase3 was detected in H460 (C/C) cells than in H460 (T/T) cells. Additionally, A549 (C/C) cells expressed higher levels of cleaved Caspase3 than the corresponding T/C cells, and the T/C cells expressed higher levels of cleaved Caspase3 than the corresponding T/T cells (Fig 1D). PARP was not involved in rs1663689-regulated cell death. In three-dimensional (3D) Matrigel culture, T/T cells formed more and larger clones than C/C cells, confirming the role of rs1663689 in cell proliferation. The spheroids formed by both T/T and C/C cells were well-polarized, characterized by a basal distribution of Laminin5 (Patarroyo *et al*, 2002), indicating that rs1663689 does not affect polarity (Fig 1E). T/T cells formed acinus in 3D culture with the loss of inner cell mass through anoikis, a type of apoptosis triggered by the loss of attachment to the extracellular matrix (Frisch, 2001). However, C/C cells were not

able to form large and hollow spheroids (Fig 1E). To explore whether T/T and C/C cells exhibit similar sensitivity to anoikis, we cultured H460 (T/T), H460 (C/C), A549 (T/T), A549 (T/C), and A549 (C/C) cells in low-attachment plates to force them into suspension and measured cell death. Suspended cells with different genotypes exhibited similar cell death in Cell Death ELISA assay and expressed comparable levels of cleaved caspase3 and PARP (Fig 1F), indicating that rs1663689 does not affect anoikis (Fig 1F). C/C cells formed significantly less colonies in soft agar than T/T cells, and each group formed less colonies than T/T cells (Fig 1G). These results collectively indicated that rs1663689 regulates proliferation and apoptosis (Fig 1B–G). In addition, the C allele was associated with lower invasion and migration (Fig 1H and I), as evaluated by the Boyden chamber assays.

To understand the molecular background underlying these behavioral changes, we studied the transcriptomic differences between H460 (T/T) and H460 (C/C) cells. Differential gene expression analysis showed that 2,017 genes were downregulated (Dataset EV1) and 1,708 genes were upregulated (Dataset EV2) in H460 (C/C) cells compared with H460 (T/T) cells. We ranked the differentially expressed genes by log<sub>2</sub>-transformed fold change values and applied gene set enrichment analysis (GSEA) to identify the differentially expressed functional gene sets (Fig 1J). The most enriched downregulated signaling pathways in H460 (C/C) cells versus H460 (T/T) cells were related to the cell cycle, including CENP-A-containing nucleosome assembly, centromere complex assembly, membrane disassembly, and nuclear envelope disassembly (Fig 1K; Dataset EV3). Specifically, *TGEBR1*, *IGFBP4*, *NEK6*, *AURKA*, *CENPF*, *LAMB1*, *CTGF*, *PTK2B*, *CCNB2*, *CDCA3*, *CDCA7*, and *CENPO* were downregulated in H460 (C/C) cells compared with H460 (T/T) cells (Fig 1L), supporting the finding that rs1663689 regulates proliferation. The most enriched upregulated signaling pathways in H460 (C/C) cells versus H460 (T/T) cells were related to protein demethylation and cholesterol storage (Dataset EV3).

### The rs1663689 variant reduces tumor growth and lung metastasis *in vivo*

To more directly study the function of rs1663689 *in vivo*, we subcutaneously injected A549 (T/T), H460 (T/T), A549 (C/C), and H460 (C/C) cells into BALB/c nude mice. Five weeks after inoculation, C/C cells formed smaller subcutaneous tumors than T/T cells, for both lines (Fig 2A–C). Immunostaining with a human Ki67 antibody showed a twofold decrease in the proportion of Ki67-positive cancer cells in C/C compared with T/T tumors (Fig 2D). In addition, when we stained subcutaneous tumor tissue sections for HLA-I, which can be used to distinguish human tumor cells from mouse cells, we observed that C/C tumors were well circumscribed with no invasion, while T/T tumors invaded the surrounding tissues (Fig 2E). Consistent with this phenotype, when we stained cells collected from the angular vein of the mice for HLA-I and tested circulating tumor cells (CTCs) using FACS, we found that mice bearing A549 (C/C) and H460 (C/C) tumors contained significantly less CTCs than those bearing A549 (T/T) and H460 (T/T) tumors (Fig 2F). Additionally, our immunostaining analysis revealed less infiltrated HLA-I-positive human cancer cell clusters in the lung tissue sections in mice bearing A549 (C/C) and H460 (C/C) tumors than in those

bearing A549 (T/T) and H460 (T/T) tumors (Fig 2G). Notably, the C/C clusters were significantly smaller than the T/T clusters, suggesting that rs1663689 also regulates proliferation in metastatic sites. To confirm the role of rs1663689 in metastatic colonization, we performed a 5-ethynyl-2'-deoxyuridine (EdU) incorporation assay. We intravenously inoculated A549 (T/T) or A549 (C/C) cells into BALB/c nude mice and analyzed lung metastasis on Days 2, 14, 28, and 42 postinjection. Immunofluorescence staining of lung sections revealed that both A549 (T/T) and (C/C) cells have settled down as small clusters in lung tissue on day 2 and followed by incremental colonization from Days 14 to 42 (Fig 2H). Compared with T/T cells, C/C cells exhibited a lower proliferative index and

therefore formed smaller metastatic clones (Fig 2H). These results indicate that rs1663689 functions in proliferation at both the primary and metastatic sites. These *in vivo* observations were consistent with the *in vitro* findings: the C genotype at rs1663689 reduces proliferation and invasion, which represses malignant lung cancer progression.

**rs1663689 is associated with lung cancer outcome**

We next assessed the rs1663689 genotype in relation to the overall survival of 239 Chinese lung cancer patients with known clinical outcomes from the Tianjin Medical University Cancer Hospital.

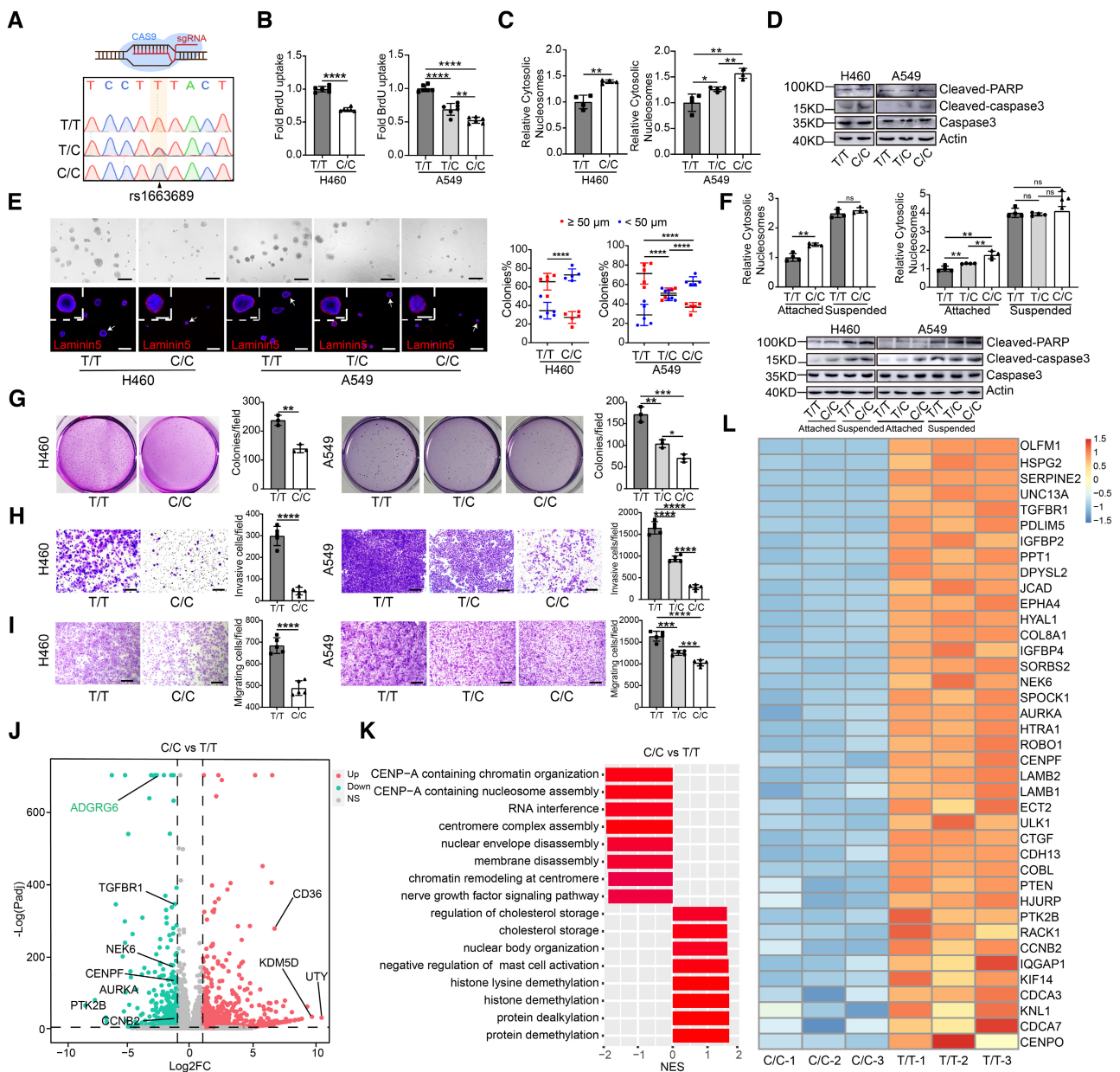


Figure 1.

**Figure 1. T allele of rs1663689 promotes cell proliferation and invasiveness.**

- A Schematic representation of the experimental strategy to mutate rs1663689 by CRISPR/Cas9 technology is shown on the top. Sanger sequencing of CRISPR/Cas9-modified cells is shown on the bottom.
- B BrdU incorporation assay for H460 and A549 cells. The mean  $\pm$  SD represents 6 biological replicates in one experiment. Three independent experiments were performed.  $**P < 0.01$ ,  $****P < 0.0001$ , unpaired two-tailed Student's *t*-test.
- C Photometric enzyme immunoassay for the qualitative and quantitative *in vitro* determination of cytoplasmic nucleosomes. The relative cytoplasmic nucleosome index for H460 and A549 cells was measured by detection with the cell death detection ELISA kit. The mean  $\pm$  SD represents 4 biological replicates in one experiment. Three independent experiments were performed.  $*P < 0.05$ ,  $**P < 0.01$ , unpaired two-tailed Student's *t*-test.
- D Immunoblot showing the expression of Cleaved-PARP, Cleaved-CASP3, CASP3, and Actin in H460 and A549 cells.
- E H460 and A549 cells were cultured in 5% Matrigel for 10 days. Representative images of the 3D Matrigel culture are shown in the top panel, and immunofluorescence staining with anti-laminin5 and DAPI is shown in the bottom panel (laminin5, red; DAPI, blue). Scale bars, 200  $\mu$ m. The right panel shows the percentages of colonies with a diameter  $\geq 50$   $\mu$ m and colonies with a diameter  $< 50$   $\mu$ m. The mean  $\pm$  SD represents 5 visual fields from one experiment. Three independent experiments were performed.  $****P < 0.0001$ , unpaired two-tailed Student's *t*-test.
- F The relative cytoplasmic nucleosome index was measured by detection with the cell death detection ELISA kit for H460 and A549 cells after 24 h under attached or suspended conditions. Immunoblot showing the expression of Cleaved-PARP, Cleaved-CASP3, CASP3, and Actin in H460 and A549 cells after 24 h under attached or suspended conditions. The mean  $\pm$  SD represents 4 biological replicates in one experiment. Three independent experiments were performed. ns, nonsignificant,  $**P < 0.01$ , unpaired two-tailed Student's *t*-test.
- G The indicated cells were allowed to grow in soft agar for 2 weeks, and colonies were counted. The mean  $\pm$  SD represents 3 biological replicates in one experiment. Three independent experiments were performed.  $*P < 0.05$ ,  $**P < 0.01$ ,  $***P < 0.001$ , unpaired two-tailed Student's *t*-test.
- H Boyden chamber assay for H460 and A549 cells. The bar chart shows the corresponding counts of invaded cells. Scale bars, 200  $\mu$ m. The mean  $\pm$  SD represents 5 visual fields from one experiment. Three independent experiments were performed.  $****P < 0.0001$ , unpaired two-tailed Student's *t*-test.
- I Images showing the motility of H460 and A549 cells by Boyden chamber assay. Scale bars, 200  $\mu$ m. The mean  $\pm$  SD represents 5 visual fields from one experiment. Three independent experiments were performed.  $***P < 0.001$ ,  $****P < 0.0001$ , unpaired two-tailed Student's *t*-test.
- J The volcano plot maps based on RNA-seq data show changes in the gene expression profile in H460 (C/C) cells versus H460 (T/T) cells.
- K Gene set enrichment analysis showed the top eight enriched pathways in H460 (C/C) cells versus H460 (T/T) cells. To the left of the column is the downregulated pathways, and the right of the column is the upregulated pathways.
- L Heatmap of differentially expressed genes identified based on RNA-seq data in H460 cells.

Source data are available online for this figure.

Patients with C/C genotype at rs1663689 exhibited moderate longer survival time than those with T/C genotype, but the benefit was not statistically significant ( $P = 0.3798$ ). Likewise, patients with T/C genotype exhibited moderate longer survival time than those with T/T genotype, but the benefit was not statistically significant either ( $P = 0.1974$ ). However, patients with C/C genotype had significantly longer survival time than those with T/T genotype ( $P = 0.0310$ , HR = 2.114) (Fig 2I and Table 1; Dataset EV4). We did not observe any association between the rs1663689 with either pathological stage or lymph node metastasis in the cohort that includes the above 239 patients (Fig 2J and Table 1; Dataset EV4).

### rs1663689 regulates ADGRG6 through interchromosomal interaction

We next sought to identify the target genes of rs1663689. Long-distance regulation requires direct physical interactions between cis-regulatory elements and their target genes through alterations in higher-order chromatin structure (Fraser & Bickmore, 2007; Zheng & Xie, 2019). Therefore, to globally screen for rs1663689-interacting DNA sequences, we conducted allele-specific circularized chromosome conformation capture followed by sequencing (4C-seq) in the heterozygous (T/C) A549 cell line using the rs1663689 region as bait (Fig 3A). We also performed chromatin immunoprecipitation followed by sequencing (ChIP-seq) for H3K4me3, a marker of promoter regions, and for H3K27ac, a marker of active enhancers and active promoters (Xia et al, 2019), to define the rs1663689-interacting DNA sequences. The commonly or differentially detected strong (top 5%) intrachromosomal /interchromosomal interactions were shown in Fig 3B and C. None of these interacting fragments

showed differential enrichment of H3K4me3 or H3K27ac, suggesting that these strong interactions are not involved in transcriptional regulation (Figs EV1 and EV2). Then, we screened all the allele-specific interacting DNA fragments from raw data of 4C for those that simultaneously showed differential enrichment of H3K4me3 and identified 13 interactions (10 C-specific and 3T-specific interactions) including 5 intrachromosomal interactions and 8 interchromosomal interactions (Dataset EV5). Among them, only ADGRG6, a C-specific interchromosomal interacting fragment that is located on chromosome 6, showed increased H3K4me3 and H3K27ac association and transcription in T/T lines versus C/C lines (Fig 3D). The other 12 fragments, however, exhibited no transcriptional difference in A549 (T/T) and A549 (C/C) cells (Fig EV3). This rs1663689C-ADGRG6 interchromosomal interaction was also detected in 4C analysis using A549 (C/C) cells but not in 4C analysis using A549 (T/T) cells (Fig 3E), and further confirmed by DNA fluorescence *in situ* hybridization (FISH) in H460 and A549 cells (colocalization percentages: 6.0% in H460 (C/C), 3.5% in H460 (T/T), 6.7% in A549 (C/C), 5.4% in A549 (T/C), 3.5% in A549 (T/T); negative control: 2.8% in H460 (C/C), 2.8% in H460 (T/T); 3.2% in A549 (C/C), 3.0% in A549 (T/C), 3.1% in A549 (T/T)) (Fig 3F). Notably, the trans contact frequency between rs1663689C and ADGRG6 is less than 10%, suggesting that this interchromosomal interaction is very dynamic, consistent with the low interacting frequency observed in 4C analysis.

Immunoblot showed that H460 cells carrying rs1663689 C/C expressed less ADGRG6 than the corresponding T/T cells. Additionally, A549 cells carrying rs1663689 C/C expressed less ADGRG6 than the corresponding T/C cells, and the T/C cells expressed less ADGRG6 than the corresponding T/T cells (Fig 3G). Consistently, expression quantitative trait locus (eQTL) analysis using data from

another cohort of 175 Chinese cancer specimens obtained from the Tianjin Medical University Cancer Hospital showed a strong association of the C allele of rs1663689 with lower *ADGRG6* transcript levels (Fig 3H; Dataset EV6). The neighboring genes of rs1663689, *GATA3*, and *CELF2*, were not altered, revealed by RNA-seq in H460 (C/C), H460 (T/T), A549 (C/C), and A549 (T/T) cells (Fig EV4A). These data indicate that rs1663689 interchromosomally regulates *ADGRG6*.

To confirm that colocalization with the rs1663689 region can repress *ADGRG6*, we inserted the rs1663689-centered 710-bp DNA sequence upstream of the *ADGRG6* promoter into a luciferase reporter construct and performed a luciferase assay. We found that

the rs1663689 region inhibited the activity of the *ADGRG6* promoter, and this repression was independent of the genotype of rs1663689 (Fig 3I). This suggests that rs1663689 resides within a silencer and that rs1663689 may regulate the proximity between the silencer and the *ADGRG6* promoter because the T and C genotypes exhibit a similar effect on the *ADGRG6* promoter when adjacent to the promoter. Taken together, these findings indicate that rs1663689C inhibits the expression of *ADGRG6* by mediating the physical interchromosomal interaction. rs1663689T fails to establish this trans contact and therefore releases the *ADGRG6* promoter from silencing (Fig 3J). However, ChIP-seq analysis showed that the reported silencer-associated histone marks, such as H3K9me3, H3K27me3, and

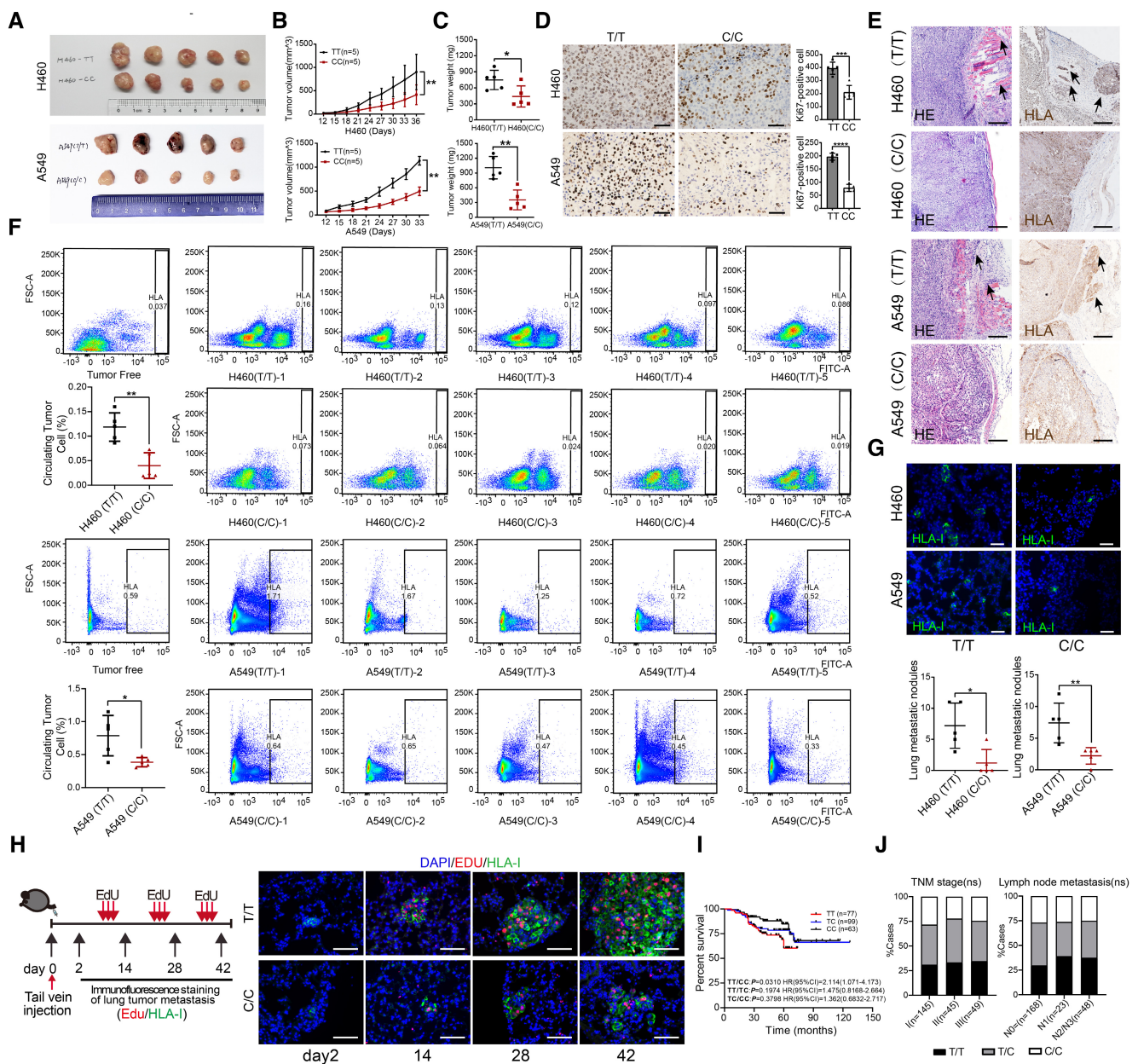


Figure 2.

**Figure 2. The T allele of rs1663689 promotes tumor growth and lung metastasis.**

- A–C H460 (T/T), H460 (C/C), A549 (T/T), and A549 (C/C) cells were subcutaneously inoculated into BALB/c nude mice ( $n = 5$ ). Primary tumors were resected after 5 weeks (A). The graphs show the mean tumor volumes (B) and weight (C). Values shown are mean  $\pm$  SD obtained from animal experiments. \* $P < 0.05$ , \*\* $P < 0.01$ , two-way ANOVA (B) and unpaired two-tailed Student's  $t$ -test (C).
- D IHC staining for Ki67 in primary tumors from animals. The panels show representative images (left), and the graph shows the quantification of Ki67-positive cells in the tumor (right). Scale bars, 100  $\mu$ m. The mean  $\pm$  SD represents 5 visual fields from each tumor tissue. \*\*\* $P < 0.001$ , \*\*\*\* $P < 0.0001$ , unpaired two-tailed Student's  $t$ -test.
- E Hematoxylin and eosin and IHC staining for HLA-I were performed in subcutaneous tumor tissue sections. The arrowhead indicates tumor cells invading surrounding tissues. Scale bars, 200  $\mu$ m.
- F The scatter plot and the percentage of HLA-I-positive circulating tumor cells (CTCs) in the peripheral blood were analyzed by flow cytometry, and numerical statistics of the two groups were calculated ( $n = 5$ ). Tumor-free mice were used as a negative control to determine the gating. \* $P < 0.05$ , \*\* $P < 0.01$ , unpaired two-tailed Student's  $t$ -test.
- G Lung sections were stained as indicated. Left, lung metastases were detected in mice inoculated with subcutaneous tumors (immunofluorescence: DAPI, blue; HLA-I, green). Scale bars, 40  $\mu$ m. Right, quantitation of lung metastatic nodules. The number of HLA-I-positive cells was counted in 5 sections per mouse. \* $P < 0.05$ , \*\* $P < 0.01$ , unpaired two-tailed Student's  $t$ -test.
- H The schematic diagram of the EdU incorporation assay and representative images of lung sections stained as indicated (immunofluorescence: DAPI, blue; HLA-I, green; EdU, red). Scale bars, 40  $\mu$ m.
- I The log-rank (Mantel-Cox) test of overall survival of 239 Chinese lung cancer patients based on rs1663689 genotype.
- J The frequency of samples of Chinese lung cancer patients with stage I–III disease and lymph node metastasis stratified by rs1663689 genotype.
- Source data are available online for this figure.

**Table 1. Patient demographics used in overall survival analysis, pathological stage, or lymph node metastasis.**

Characteristic	All patients (n = 239)	T/T (n = 77)	T/C (n = 99)	C/C (n = 63)
Age at treatment				
Mean $\pm$ SD	60.4 $\pm$ 8.1	60.6 $\pm$ 7.5	60.2 $\pm$ 8.0	60.4 $\pm$ 8.1
Median (range)	62 (30–74)	62 (34–74)	62 (34–70)	62 (30–74)
Sex, no. (%)				
Female	111 (46)	43 (56)	41 (42)	27 (43)
Male	128 (54)	34 (44)	58 (58)	36 (57)
Primary diagnosis, no. (%)				
LUAD	179 (75)	64 (83)	68 (69)	47 (75)
LUSC	47 (20)	10 (13)	23 (23)	14 (22)
LCC	6 (2)	1 (1)	5 (5)	0 (0)
SCLC	7 (3)	2 (3)	3 (3)	2 (3)
Survival, no. (%)				
Survive	181 (76)	53 (69)	76 (77)	52 (83)
Death	58 (24)	24 (31)	23 (23)	11 (17)
TNM stage, no. (%)				
I	145 (61)	45 (59)	59 (60)	41 (65)
II	45 (19)	15 (19)	20 (20)	10 (16)
III	49 (20)	17 (22)	20 (20)	12 (19)
Lymph node metastasis, no. (%)				
NO	168 (70)	50 (65)	73 (74)	45 (71)
N1	23 (10)	9 (12)	8 (8)	6 (10)
N2/N3	48 (20)	18 (23)	18 (18)	12 (19)

LCC, large cell carcinoma; LUAD, adenocarcinoma; LUSC, squamous cell adenocarcinoma; SCLC, Small-small-cell lung carcinoma.

H3K27ac (Rea *et al*, 2000; Heintzman *et al*, 2007; Campos & Reinberg, 2009; Pang & Snyder, 2020), were not enriched in this rs1663689-encompassing DNA fragment (Fig EV4B).

**ADGRG6 is involved in rs1663689-regulated proliferation and invasion**

ADGRG6 is a member of the adhesion GPCR family and mediates cell-extracellular matrix interactions with type IV collagen and prior protein as its agonistic ligand (Fredriksson *et al*, 2003; Bjarnadottir *et al*, 2004; Paavola *et al*, 2014; Hamann *et al*, 2015; Petersen *et al*, 2015; Küffer *et al*, 2016). ADGRG6 is crucial for development and its germline mutations or somatic mutations are associated with multiple developmental diseases in humans (Hancock *et al*, 2010; Kou *et al*, 2013; Ravenscroft *et al*, 2015; Shaffer *et al*, 2017; Hosseini *et al*, 2019). To explore whether ADGRG6 is involved in rs1663689-regulated proliferation and invasion, we knocked down ADGRG6 in H460 (T/T) and A549 (T/T) cells and overexpressed ADGRG6 in H460 (C/C) and A549 (C/C) cells and analyzed the proliferation and invasion phenotypes of the resulting cells (Fig 4A). ADGRG6 knock-down in T/T cells decreased the proliferative index and invasive capability to the levels seen in the corresponding C/C cells, whereas ADGRG6 overexpression in C/C cells enhanced the proliferative index and invasive capability to the levels seen in the corresponding T/T cells (Fig 4B and C). These results indicate that ADGRG6 greatly contributes to rs1663689-regulated proliferation and invasion. Thus, our study identifies a noncoding SNP that is involved in a long-range interaction underlying ADGRG6 transcriptional regulation. Compared with intrachromosomal interactions, many fewer interchromosomal interactions are known. Interchromosomal interactions are mostly involved in promoting the formation of chromatin domains such as centromere clusters and the nucleolus or controlling X chromosome inactivation (Bacher *et al*, 2006; Xu *et al*, 2006; Splinter & de Laat, 2011; Quinodoz *et al*, 2018; Muller *et al*, 2019; Nedeljkovic & Sundberg, 2020). Our study demonstrates the pathologic significance of interchromosomal interactions.

**The PKA inhibitor H89 reduces the growth of patient-derived organoids carrying the homozygous T/T genotype at rs1663689**

ADGRG6 signals through G $\alpha$  proteins to transiently elevate cyclic adenosine monophosphate (cAMP) and activate PKA in Schwann

cells (Moriguchi *et al*, 2004; Stehlik *et al*, 2004; Pogoda *et al*, 2006; Monk *et al*, 2009, 2011; Glenn & Talbot, 2013; Mogha *et al*, 2013, 2016; Paavola *et al*, 2014). Because tumor cells carrying the homozygous T/T genotype express higher levels of ADGRG6 than cells with other genotypes, we expected that these cells would exhibit relatively higher PKA activity. Indeed, the level of PKA substrate phosphorylation in A549 (T/T) cells was higher than that in A549 (T/C) cells, and the level of PKA substrate phosphorylation in A549 (T/C) cells was higher than that in A549 (C/C) cells. Similarly, the level of PKA substrate phosphorylation in H460 (T/T) cells was higher than that in H460 (C/C) cells (Fig 5A). We next explored the responses of

H460 and A549 cells carrying different rs1663689 genotypes to the PKA inhibitor H89 [N-[2-p-bromocinnamylamino-ethyl]-5-isoquinolinesulfonamide], a compound that blocks PKA actions through competitive inhibition of the adenosine triphosphate site on the PKA catalytic subunit (Lochner & Moolman, 2006; Fig 5A). As expected, H89 treatment significantly impaired the proliferation and invasion of H460 and A549 cells carrying the homozygous T/T genotype of rs1663689 (Fig 5B and C). However, H89 treatment had little effect in both cell lines carrying the homozygous C/C genotype of rs1663689 (Fig 5B and C). To further confirm that targeting PKA may benefit lung cancer patients carrying the T/T genotype at

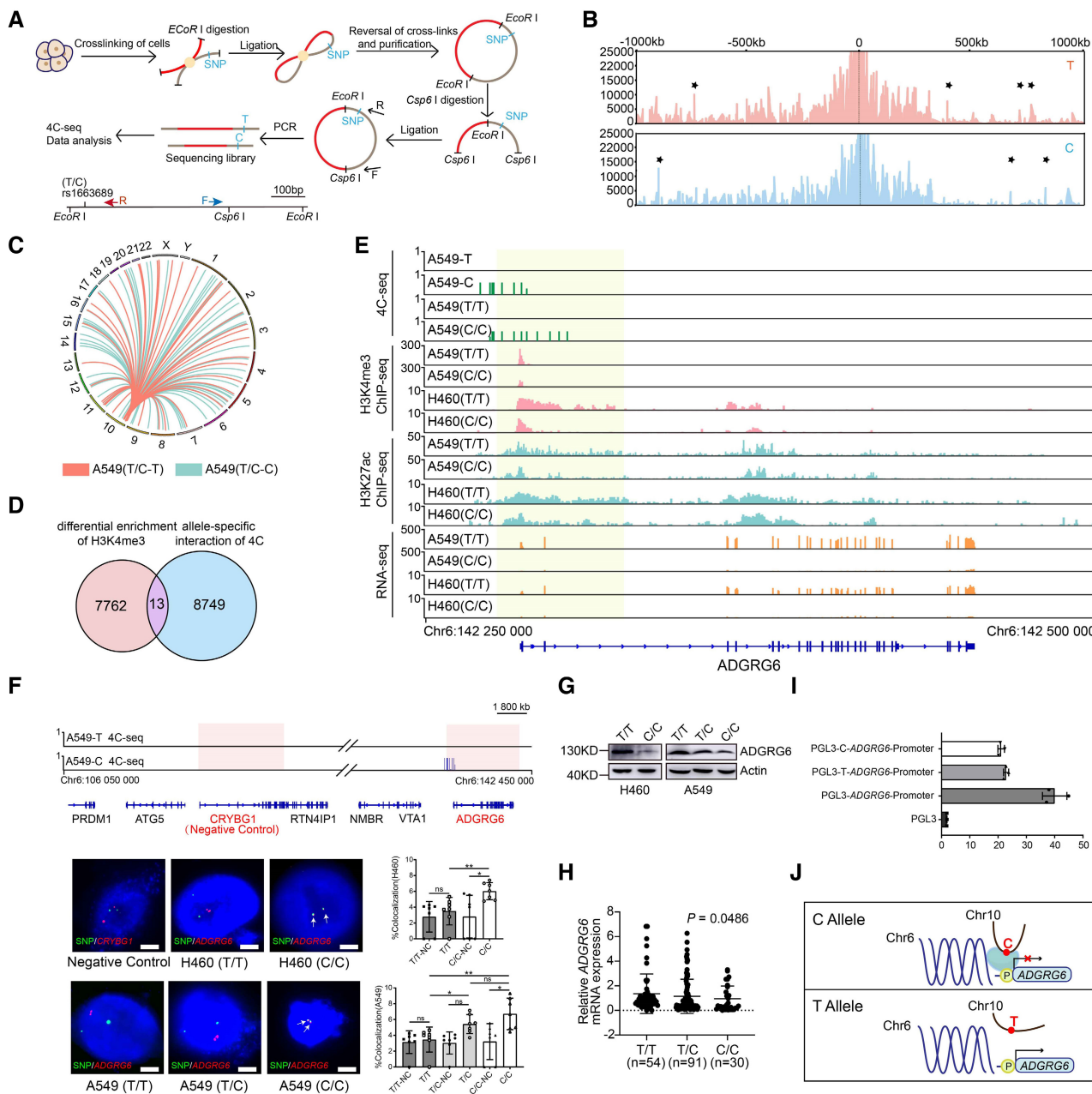
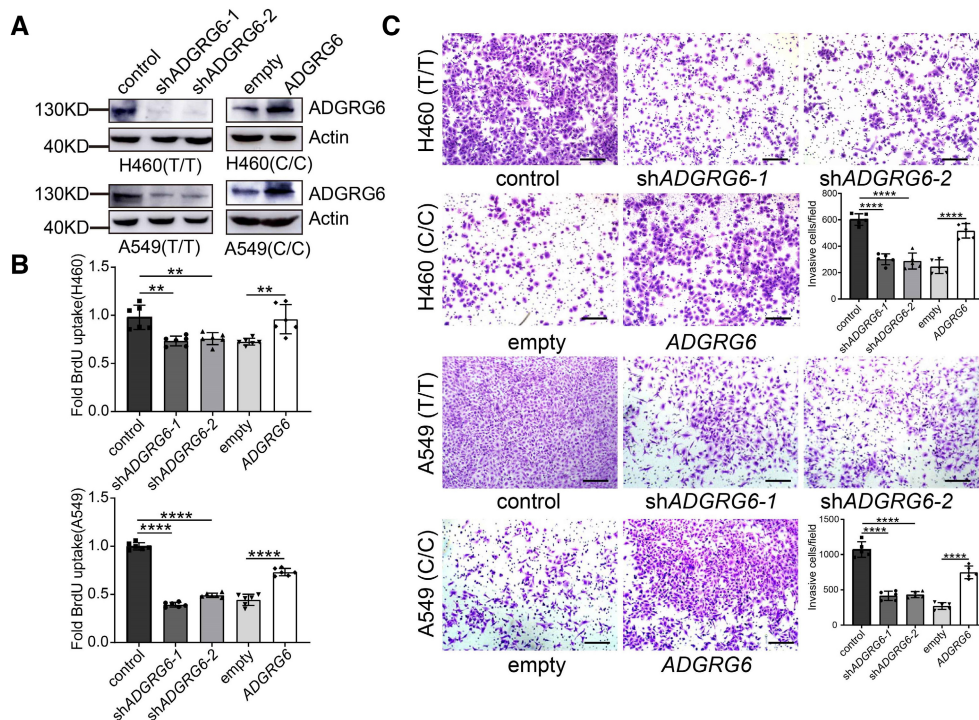


Figure 3.

**Figure 3. rs1663689 regulates ADGRG6 through interchromosomal interaction.**

- A Flow chart of 4C technology.
- B The panel shows the intrachromosomal interactions within 2 Mb around the central position of rs1663689 (T/C). 4T-specific and 3 C-specific intrachromosomal interactions were marked with asterisks above them. The axes label of 2 Mb scales is chr10:7980000–9980000.
- C Circos plot for intrachromosomal interactions and interchromosomal interactions in T allele-specific 4C compared with C allele-specific 4C of A549 (T/C) cells as detected from broad domain analysis using domainograms.
- D Venn diagram showing the degree of overlap between allele-specific interacting DNA fragments in raw data of A549 (T/C) cells and the specific enrichment of H3K4me3 peak of A549 (T/T) cells and A549 (C/C) cells.
- E 4C-seq distribution map showing specific peaks in A549 (T/C) cells, A549 (T/T) cells and A549 (C/C) cells, H460 (T/T) and H460 (C/C) cells. The yellow shade indicates the *ADGRG6* promoter.
- F The location diagram shows 4C enrichment around the negative control and *ADGRG6* probe. Representative images of nuclei stained with DNA FISH probes for SNP rs1663689 (green) and negative control (red) or *ADGRG6* (red) in H460 and A549 cells. The numerical points in the figure show the percentage of colocation in seven slides (with a total of 80 nuclei). Arrows point to the colocation signals. Nuclei with a green or red positive signal are listed in the counting range. Values shown are mean  $\pm$  SD. Scale bars, 5  $\mu$ m. ns, nonsignificant, \* $P < 0.05$ , \*\* $P < 0.01$ , unpaired two-tailed Student's *t*-test.
- G Expression of *ADGRG6* at the protein levels in H460 and A549 cells.
- H eQTL analysis demonstrating the correlation between the rs1663689 genotype and the expression of *ADGRG6* in the clinical patient cohorts. The *P*-value of the linear model was assessed by the Kruskal–Wallis test. Values shown are mean  $\pm$  SD.
- I Luciferase reporter activity is shown with pGL3-basic vector, vector with *ADGRG6* promoter, and vector with a 710-bp SNP-centered sequence inserted upstream of the promoter. The mean  $\pm$  SD represents 3 biological replicates in one experiment. Three independent experiments were performed.
- J Graphical representation of the role of the noncoding SNP rs1663689 in regulating interchromosomal interaction. rs1663689 resides within a silencer, and the C allele promotes an interchromosomal interaction between the silencer and *ADGRG6* promoter, which inhibits the expression of *ADGRG6*. rs1663689T fails to establish this trans contact and therefore releases the *ADGRG6* promoter from silencing, which increases *ADGRG6* expression.

Source data are available online for this figure.

**Figure 4. ADGRG6 is involved in rs1663689-regulated proliferation and invasion.**

- A Protein expression of *ADGRG6* or Actin after *ADGRG6* knockdown in T/T cells and overexpression in C/C cells.
- B, C BrdU incorporation assay (B) and Boyden chamber assay (C) of *ADGRG6*-knockdown T/T cells and *ADGRG6*-overexpressing C/C cells. Values shown are mean  $\pm$  SD obtained from one experiment. Scale bars, 200  $\mu$ m. Three independent experiments were performed. \*\* $P < 0.01$ , \*\*\*\* $P < 0.0001$ , unpaired two-tailed Student's *t*-test.

Source data are available online for this figure.

rs1663689, we used patient-derived organoids (PDOs). We collected 15 fresh human primary lung cancer tissues (tumor 1: T/T; tumor 2: T/T; tumor 3: T/T; tumor 4: T/T; tumor 5: T/C; tumor 6: T/C;

tumor 7: T/C; tumor 8: T/C; tumor 9: T/C; tumor 10: T/C; tumor 11: T/C; tumor 12: T/C; tumor 13: T/C; tumor 14: C/C; tumor 15: C/C, Table EV1), dissociated the cancer tissues into individual



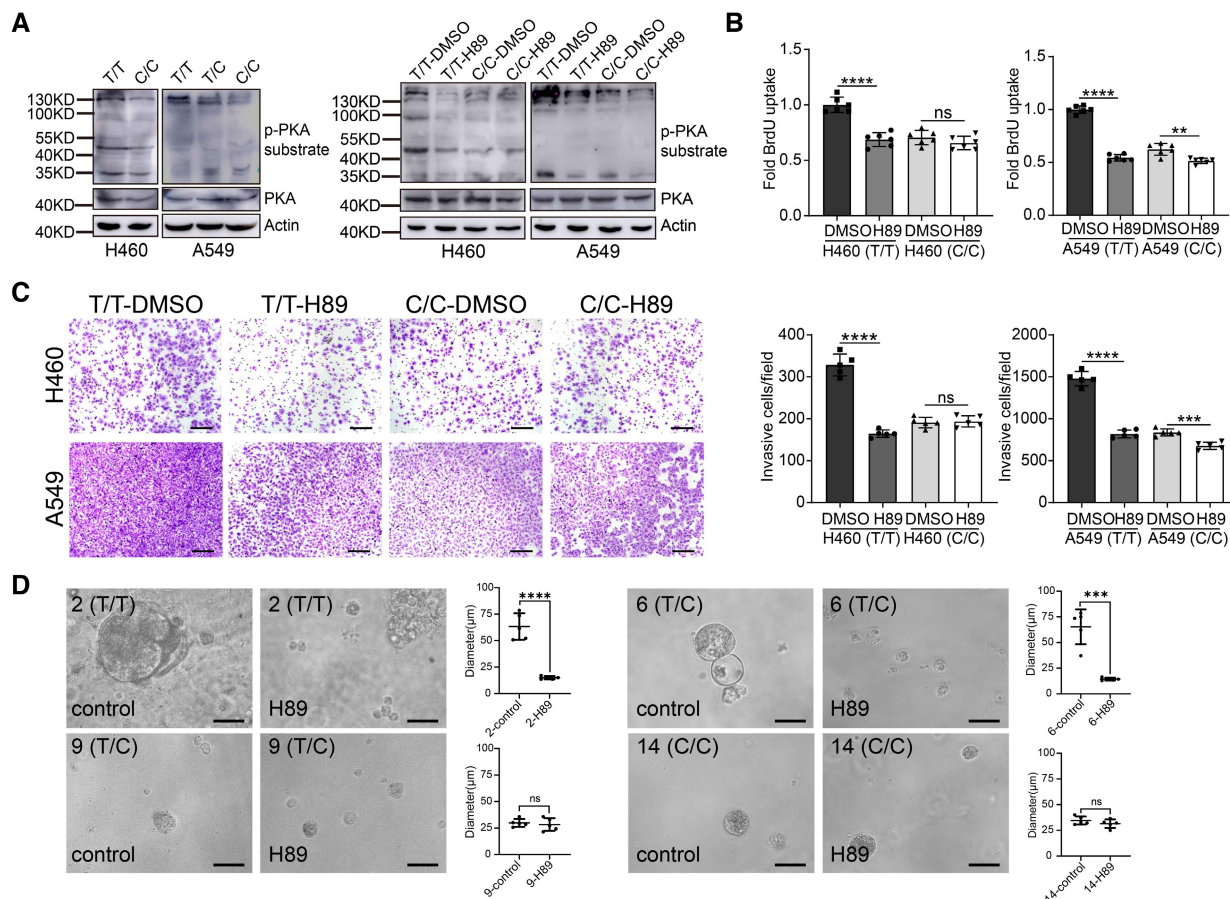


**Figure 5. H89 exhibited a significantly repressive effect on the proliferation and invasiveness of cancer cells and impaired the growth of patient-derived organoids (PDOs) harboring the homozygous T genotype at rs1663689.**

**A** Immunoblot showing the expression of PKA substrate phosphorylation, PKA, and Actin in the indicated cells and genotypes and the indicated cells treated with H89.

**B, C** BrdU incorporation assay (**B**) and Boyden chamber assay (**C**) of the indicated cells after treatment with H89. Scale bars, 200  $\mu$ m. Values shown are mean  $\pm$  SD obtained from one experiment. Three independent experiments were performed. ns, nonsignificant, \*\* $P < 0.01$ , \*\*\* $P < 0.001$ , \*\*\*\* $P < 0.0001$ , unpaired two-tailed Student's *t*-test.

**D** Representative images and quantification of patient-derived organoids treated with 20  $\mu$ M H89 and controls. The mean  $\pm$  SD represents 5 visual fields from one experiment. Scale bars, 20  $\mu$ m. ns, nonsignificant, \*\*\* $P < 0.001$ , \*\*\*\* $P < 0.0001$ , unpaired two-tailed Student's *t*-test.

Source data are available online for this figure.

cells or cell clusters, and cultured them in 3-dimensional Matrigel containing necessary factors, as described previously (Kim *et al.*, 2019). Except for tumor 1 (T/T) and tumor 5 (T/C), the other 13 tumors successfully developed organoids in the 3-dimensional Matrigel. Notably, the 3 tumors carrying the T/T genotype at rs1663689 developed larger organoids than the tumors carrying the T/C or C/C genotype at rs1663689 (Figs 5D and EV5), supporting the above results showing that T is associated with elevated proliferation and reduced apoptosis. In addition, while H89 exhibited a significant repressive effect on the growth of all T/T organoids, it had no effect on C/C organoids (Figs 5D and EV5). T/C organoids from different lung cancer patients exhibited differential responses to H89. Organoids from tumors 6, 7, and 8 were repressed by H89, whereas organoids from tumors 9, 10, 11, 12, and 13 were not responsive to H89 (Figs 5D and EV5). These PDO data confirm that rs1663689 may be predictive of cAMP-PKA dependency in lung cancers, which suggests that targeting *ADGRG6* or the cAMP-PKA

signaling pathway may benefit lung cancer patients with the T/T genotype at rs1663689.

How rs1663689 regulates *ADGRG6* is not defined in this study. Presumably, rs1663689 regulates the binding affinity of a transcription factor that directly or indirectly controls the physical interchromosomal interaction between the SNP and *ADGRG6*. Identifying this transcription factor and deciphering the molecular mechanisms underlying interchromosomal interaction formation will be an interesting future study.

## Materials and Methods

### Human samples

The lung cancer tissues used in this study were all from the Tianjin Medical University Cancer Hospital. Informed consent of patients

was obtained before use, and samples were deidentified before analysis. The relevant experiments were approved by the Institutional Review Committee of Tianjin Medical University.

### Cell culture

A549, H460, and HEK293T cells were purchased from ATCC. A549 and H460 cells were cultured with 10% FBS-RPMI 1640 (GIBCO), and HEK293T cells were cultured with 10% FBS-DMEM (GIBCO). All cells were cultured at 37°C under a humidified atmosphere containing 5% CO<sub>2</sub>.

### SNP editing with CRISPR/Cas9

Single guide RNAs (sgRNAs) that bind near rs1663689 were designed with an online tool (<http://crispr.mit.edu/>) and cloned into pX458, which expressed green fluorescent protein and Cas9 (Addgene, pSpCas9(BB)-2A-GFP, Plasmid 48138). A 68 bp double-stranded DNA (dsDNA) containing “T” or “C” at rs1663689 was used for homology-directed repair. A total of 4 µg pX458 containing sgRNAs and 14 pmol of dsDNA donor were cotransfected into A549 and H460 cells in 60 mm culture dishes following the instructions of the Lipofectamine™ 3000 Reagent Protocol (1684916, Thermo Fisher). Thirty-six hours after transfection, FACS sorting was carried out using the expression of GFP as a selection marker. Single cells were cultured in 96-well plates to form clones. Genomic DNA was extracted using a Genomic DNA Purification Kit (EE101-02, TransGen) according to the manufacturer’s instructions. The rs1663689 region was amplified by PCR and verified by Sanger sequencing. Primers were listed in Table EV2.

### BrdU cell proliferation assays

For the cell proliferation assays,  $1.5 \times 10^3$  cells were cultured in 96-well plates for 24 h. 5-Bromo-2'-deoxyuridine was added according to the manufacturer’s instructions, Cell Proliferation ELISA (11647229001, Roche). The absorbance was measured at 450 nm on an enzyme-labeled instrument.

### Cell death ELISA assay

The apoptosis of A549 and H460 was assessed by Cell Death Detection ELISA PLUS kit (11774425001, Roche) following the manufacturer’s instructions. Briefly,  $5 \times 10^4$  cells were cultured in 24-well plates for 24 h. Cells were harvested and lysed with 200 µl lysis buffer for 30 min at room temperature, followed by centrifuging at 200 g for 10 min. Twenty microlitre of the supernatant that contains histone-associated DNA fragments was added into streptavidin-coated microplate. Anti-Histone-Biotin and Anti-DNA-POD were then added into the microplate for 90 min at room temperature. After washing 3 times with incubation buffer, POD was determined photometrically with 100 µl ABTS substrate. The absorbance was read at 405 nm on an ELISA microplate reader. For anoikis determination, cells were cultured on ultralow-attachment 24-well plates for 24 h and harvested for cell death detection.

### 3D Matrigel culture

The growth factor-reduced Matrigel (Corning) was thawed at 0°C overnight. Matrigel was diluted to 5% with prechilled 2% FBS-RPMI 1640 medium. Cells were trypsinized, centrifuged, resuspended, counted, and diluted with 5% Matrigel-RPMI 1640 to  $4 \times 10^3$ /ml, and 500 µl of cell mixture was added to each well of 24-well ultralow-attachment plates (Corning). Cells were incubated at 37°C and 5% CO<sub>2</sub> for 8–10 days. The culture was replenished with 100 µl of 5% Matrigel-RPMI 1640 every 2 days.

### Soft agar colony formation

A two-layer soft agar system in 6-well plates was used. The lower layer contained 10% FBS-RPMI 1640 and 0.6% agar, and the upper layer contained  $1 \times 10^4$  cells in a final volume of 1 ml of 10% FBS-RPMI 1640 and 0.35% agar. The system was replenished with 200 µl of 10% FBS-RPMI 1640 every 3 days. After 2 weeks of incubation, the dishes were stained with 0.005% crystal violet for 3 h, and the numbers of colonies were quantified using ImageJ software.

### Cell invasion assays

Twenty-four-well plates were used for this assay. A 500 µl volume of 10%-FBS culture medium was added to each well before transferring Transwell inserts with 8 µm membrane (BD Biosciences) coated with 20% Matrigel (Corning). A total of  $2 \times 10^5$  cells suspended in serum-free medium were plated into the upper chamber of the Transwell inserts. After incubation at 37°C and 5% CO<sub>2</sub> for 20 h, the cells that had invaded through the membrane to the lower surface were fixed with 4% paraformaldehyde for 15 min, stained with 0.1% crystal violet for 10 min, and washed three times with PBS. Images were captured under an inverted microscope.

### Migration assays

Twenty-four-well plates were used for this assay. The lower surface of Transwell inserts with 8 µm membrane (BD Biosciences) was precoated with 100 µg/ml poly-L-lysine (P4707, Sigma) at room temperature for 10 min. The Transwell inserts were washed three times with sterile water, and then coated with 50 µg/ml Laminin (L2020, Sigma) at 37°C for 30 min and washed three times with PBS before use. A 500 µl volume of 10%-FBS culture medium was added to each well before transferring Transwell inserts. A total of  $2 \times 10^5$  cells suspended in 0.1% FBS-RPMI 1640 medium were plated into the upper chamber of the Transwell inserts. After incubation at 37°C and 5% CO<sub>2</sub> for 24 h, the cells that had migrated through the membrane to the lower surface were fixed with 4% paraformaldehyde for 15 min, stained with 0.1% crystal violet for 10 min, and washed three times with PBS. Images were captured under an inverted microscope.

### Xenograft assay and circulating tumor cells experiments

Animal studies were approved by the Tianjin Medical University Animal Care and Use Committee. All mice were maintained under

specific pathogen-free conditions. H460 cells ( $2 \times 10^5$ ) mixed with human lung CAFs ( $1 \times 10^5$ ) and A549 cells ( $6 \times 10^5$ ) mixed with human lung CAFs ( $3 \times 10^5$ ) in 100  $\mu$ l PBS containing Matrigel (1:1 vol/vol; Corning) were inoculated subcutaneously into BALB/c nude mice (36 and 33 days). Tumor size was measured every 3 days using calipers with a Vernier scale. Tumor volume was calculated as (length  $\times$  width  $\times$  width)/2. For the circulating tumor cells (CTCs) assay, 1 ml blood from each mouse was collected into EDTA tubes and diluted with 1 ml PBS. The tumor cells were enriched using Ficoll centrifugation at 500 rpm for 30 min at room temperature. The cells were washed in 10 ml PBS, and ACK was used for erythrocyte lysis. CTCs were detected using an HLA antibody (1:200) and a FITC-conjugated secondary antibody (1:200). DAPI was used to exclude dead cells. Then, the cells were analyzed by flow cytometry.

### EdU incorporation experiments

For the EdU incorporation assay, viable A549 cells ( $2 \times 10^6$ ) were resuspended in 100  $\mu$ l PBS and injected into the tail vein of 5-week-old female BALB/c nude mice. Three days before sacrifice on days 14, 28, or 42, mice were intraperitoneally injected with EdU at 400  $\mu$ g/day (the mice that were sacrificed on day 2 were not given EdU). Lung sections were processed for immunofluorescent detection of HLA and EdU.

### Immunohistochemistry

Mouse tumor and lung tissues were fixed in 4% paraformaldehyde overnight at 4°C and embedded in paraffin. Paraffin-embedded tissues were cut into 5  $\mu$ m sections. After dewaxing and rehydration, the tissues were repaired and then washed with PBS followed by permeabilization and blocking for 1 h and then staining with antibodies against HLA-I (ab70328, Abcam) following standard DAB staining protocols.

### Immunofluorescence

Spheroids harvested from the 3D culture were transferred to slides and air-dried. The slides were fixed with 2% PFA and successively washed three times with 0.1% BSA in PBS and 0.75% glycine in PBS. Then, slides were sequentially blocked with 10% normal goat serum (NGS) and Fab (1:100) at room temperature for 1 h. The slides were then incubated with laminin5 (ab78286, Abcam) primary antibody (1:200) at 4°C overnight. On the next day, the slides were incubated with goat anti-mouse secondary antibody (A21422, Thermo Fisher) for 1 h and sealed with a DAPI-containing medium. To examine lung metastases of subcutaneous tumors in mice, paraffin sections of lung tissue were incubated with HLA-I primary antibodies (1:100) at 4°C overnight and then with goat anti-mouse (A11001, Thermo Fisher) secondary antibody (1:500) for 1 h at room temperature.

### Gene expression analysis by qPCR and eQTL

Lung cancer tissues were collected from patients at Tianjin Medical University Cancer Hospital, and informed consent was obtained from all patients. For genomic DNA extraction, samples were subjected to a kit following the manufacturer's protocol and genotyping by

Sanger sequencing. For total RNA extraction, tissues were cut into small pieces, and RNA was isolated by TRIzol (15596026, Thermo Fisher) and chloroform, precipitated with isopropanol, and washed with 75% ethanol. cDNAs were synthesized from 2  $\mu$ g of total RNA using oligo(dT) with the RevertAid First Strand cDNA Synthesis Kit (11483188001, Thermo Fisher). The mRNA expression of *ADGRG6* was measured by RT-qPCR, which was performed using SYBR Green Master Mix (DBI-2043, DBI® Bioscience). Primers were listed in Table EV2.

### 4C-sequencing analysis

4C-seq was performed as previously described using *EcoR* I for the first digestion and *Csp6* I for the second digestion. In brief, cells were cross-linked in 2% formaldehyde for 10 min at room temperature, and glycine (V900144, Sigma) was added to a final concentration of 0.2 M to quench the reaction. After crosslinking, the cells were rinsed twice with cold PBS at room temperature and incubated in lysis buffer (50 mM Tris-Cl, pH 8.0, 150 mM NaCl, 5 mM EDTA, 0.5% CA630, 0.1% Triton X-100 and protease inhibitor cocktail [04693132001, Roche]) with rotation for 1 h at 4°C. Cells were then pelleted, washed, and resuspended in *EcoR* I buffer. SDS was added to a final concentration of 0.3% for 1 h in a thermomixer at 37°C and 900 rpm. Triton X-100 was then added to a final concentration of 1.8% and incubated in a thermomixer at 37°C and 900 rpm for 3 h. Two hundred units of *EcoR* I enzyme (New England Biolabs, R3101M) were added for a 4 h incubation in a thermomixer at 37°C and 900 rpm; another 200 units of *EcoR* I were added for overnight incubation. *EcoR* I was heat-inactivated by incubation at 65°C for 20 min. Cells were suspended in a ligation buffer, to which 4,000 units of T4 ligase (New England Biolabs, M0202M) were added and incubated for more than 8 h at 16°C and 300 rpm. After ligation, 300  $\mu$ g Proteinase K was added for overnight incubation at 65°C and 400 rpm. DNA was purified and digested with 90 units of *Csp6* I (New England Biolabs, R0639S) and incubated for 5 h in a thermomixer at 25°C and 500 rpm, followed by heat inactivation of the enzyme at 65°C for 20 min. DNA was then diluted with ligation buffer, and 100 units of T4 ligase were added for ligation overnight at 16°C and 300 rpm. The product of the second ligation, that is, circularized DNA, was purified and amplified using bait-specific inverse primers (29 bp downstream of rs1663689 and 55 bp downstream of the *EcoR* I site) to identify the allele at the SNP and unknown DNA sequences interacting with the bait. Primers were extended with overhanging Illumina adaptor sequences. After amplification, the PCR products were pooled and purified. Sequencing reads were demultiplexed and trimmed of the primer sequence using the saber tool (<https://github.com/najoshi/sabre>), mapped to the human reference genome (hg38) with Bowtie2 (version 2.2.1) and converted to restriction fragment space. The 4C data were analyzed by pipe4C using a sliding window size of 0, then merged any fragment within 2,000 bp using bedtools. The reads number was ranked for all interactions and selected the top 5% of intrachromosomal interactions and the top 5% of interchromosomal interactions for visualization.

### Chromatin immunoprecipitation sequencing (ChIP-seq)

This assay was performed as previously described. A total of  $1 \times 10^7$  cells were cross-linked in culture media containing 1% formaldehyde

(preheated to 37°C) for 10 min at room temperature and then quenched with 0.125 M glycine (V900144, Sigma) for 5 min. Cells were washed twice with PBS and harvested in SDS Buffer (100 mM NaCl, 50 mM Tris-Cl, pH 8.1, 5 mM EDTA, 0.5% SDS, and protease inhibitor cocktail). After that, the cells were centrifuged at 500 g and 4°C for 10 min and resuspended in precooled IP Buffer (IP buffer = 1 volume SDS Buffer: 4 volume Triton Dilution Buffer [100 mM Tris-Cl, pH 8.0, 100 mM NaCl, 5 mM EDTA, pH 8.0, 1.25% Triton X-100]) for sonication. The sonication settings were as follows: 10 s on, 20 s off, 8 min of total sonication time, and amplitude 45%. Samples were rotated at 4°C overnight with 6 µg of antibodies (H3K4me3 [ab8580, Abcam], H3K27ac [ab4729, Abcam]). Antigen-antibody complexes were collected with protein A Sepharose beads (17-0618-01, GE Healthcare) rotating at 4°C for 6 h followed by centrifugation at 1,800 g and 4°C for 1 min. Beads were sequentially washed with low-salt buffer (0.1% SDS, 1% Triton X-100, 150 mM NaCl, 2 mM EDTA, pH 8.0, 20 mM Tris-Cl, pH 8.0) and high-salt buffer (0.1% SDS, 1% Triton X-100, 500 mM NaCl, 2 mM EDTA, pH 8.0, 20 mM Tris-Cl, pH 8.0). The beads were then resuspended in elution buffer (1% SDS, 0.1 M NaHCO<sub>3</sub>, and cocktail) and incubated at 65°C overnight with shaking to elute DNA and reverse the crosslinking. Supernatants containing DNA were purified with a MinElute PCR Purification Kit (28106, QIAGEN) for sequencing library preparation. Trimmed reads from the sequence were mapped to a restriction-digested human reference genome (hg38) using Bowtie2 (version 2.2.1). The allele-specific interacting DNA fragments were screened from raw data of 4C for those that simultaneously showed allele-specific enrichment of H3K4me3. Peak calling of the H3K4me3 ChIP-seq was conducted using MACS (v2.1.4). The differential peaks were detected by Bioconductor packages edgeR and compared with all allele-specific 4C contacts. Integrative Genomics Viewer (IGV) was used to generate and visualize ChIP-seq tracks.

### RNA sequencing

After the cell culture medium was discarded, TRIzol (15596026, Thermo Fisher) was added to extract RNA. Three replicates for each sample were submitted to Novogene for RNA sequencing. The barcode sequence library was constructed using a TruSeq RNA Sample Preparation Kit (Illumina) and sequenced on a NovaSeq 6000 instrument.

### Luciferase assays

Segments surrounding rs1663689 and the promoter of *ADGRG6* were cloned into the multiple cloning site of the pGL3-basic vector and verified by Sanger sequencing. 293 T cells were cultured in 10% FBS-DMEM until ready for transfection. Luciferase plasmids were cotransfected into 293 T cells with the Renilla plasmid pRL-TK as a control using Lipofectamine 3000 (1684916, Thermo Fisher). After 24 h, firefly and Renilla luciferase activities were measured using the Dual-Luciferase Reporter Assay System (E1960, Promega) according to the manufacturer's protocol.

### DNA fluorescence *in situ* hybridization

DNA FISH was performed as previously described. DNA probes targeting the *ADGRG6* promoter and the SNP were amplified from

A549 genomic DNA. The probes targeting *CRYBG1*, which did not interact with rs1663689 were used as a negative control. To synthesize the biotin- and digoxigenin-labeled dUTP probe, 1 µg DNA was labeled at 16°C overnight using a Nick Translation Kit (10976776001, Roche) as described by the manufacturer's protocol. Labeled DNA was precipitated with salmon sperm DNA (15632-011, Thermo Fisher) and human Cot-1 DNA (15279-001, Thermo Fisher) at -20°C for more than 3 h, followed by centrifugation at 4°C for 30 min. The probe DNA was washed twice with 75% ethanol and successively dissolved at 37°C with formamide (11814370001, Roche) for 30 min and a dextran sulfate mixture for 10 min. After 24 h of incubation, cells on the slide were fixed with 4% paraformaldehyde. The slide was successively immersed in 0.1 M Tris-Cl (pH 7.4), 0.1% Triton X-100 in PBS, PBS for 10 min, and 20% glycerol in PBS for 30 min at room temperature. The slide was repeatedly freeze-thawed with liquid nitrogen five times and then washed twice with PBS for 5 min at room temperature. The slide was then washed with 0.1 M HCl for 30 min, PBS for 10 min, 0.5% Triton X-100 in PBS for 30 min, and PBS again. Before hybridization, the DNA in the cells on the slide was denatured in 50% formamide in 2 × SSC (F3369, Sigma, pH 7.0) for 1 h. Subsequently, the hybridization buffer-containing probe DNA was added to the sample area of the slide, covered with glass, and sealed. The material on the slide was denatured at 85°C for 10 min, followed by hybridization at 37°C in a humidified chamber. Forty-eight hours later, the slide was successively immersed in 50% formamide in 2 × SSC at 45°C for 15 min, 0.2 × SSC at 63°C for 15 min, 2 × SSC at 45°C for 5 min, and 2 × SSC at room temperature for 5 min. Thereafter, the cells were blocked with 4% BSA in 4 × SSC at room temperature for 1 h and incubated with antibodies against biotin (ab201341, Abcam) and digoxigenin (ab64509, Abcam; both 1:200) at 4°C overnight. The next day, goat anti-mouse (A21422, Thermo Fisher) and donkey anti-sheep (ab150177, Abcam) secondary antibodies were applied. After that, DAPI was applied to the cell area and covered with a coverslip.

### Immunoblots

2 × Laemmli sample buffer containing β-mercaptoethanol (BIO-RAD) was used for protein extraction. Proteins were separated by 10% Bis-Tris gels using 1 × SDS running buffer and transferred to PVDF membranes. Blots were blocked in TBS containing 5% milk and incubated overnight with ADGRG6 (CSB-PA002757, CUSABIO), PKA (AF7746, Affinity), p-PKA substrate (9624S, Cell Signaling Technology), and actin (AC026, ABclonal) antibodies. The next day, blots were washed three times with TBS containing 1% Tween and exposed to the secondary antibody for 1 h at room temperature. Blots were washed three times followed by incubation in luminol-based substrate for HRP-catalyzed detection. Luminescence was captured on an Amersham Imager 600.

### Gene knockdown and overexpression

For gene knockdown, shRNA sequences targeting *ADGRG6* were designed with an online tool (<https://rnaidesigner.thermofisher.com/rnaexpress/sort.do>) and cloned into the pSUPER.retro.puro vector. The shRNA sequence together with the H1 promoter was inserted into the lentiviral shuttle vector pCCL.PPT.hPGK.GFP.Wpre. For gene

overexpression, the *ADGRG6* CDS was amplified from H460 cDNA and cloned into pCCL.PPT.hPGK.IRES.GFP/pre. Primers were listed in Table EV2. Then, the lentivirus was packaged in HEK293T cells with the pMD2.BSBG, pMDLg/pRRE, and pRSV-REV packaging plasmids and used to infect H460 and A549 cells. Gene expression was detected by qPCR and western blotting.

### PKA inhibitor treatment

H460 and A549 cells were cultured in an appropriate medium supplemented with DMSO or 20  $\mu$ M PKA inhibitor H89 (S1582, Selleck Chemicals). The cells were kept in the presence of H89 for 24 h and then harvested for protein extraction and subsequent phenotypic experiments.

### Patient-derived organoids culture

Lung cancer samples from Tianjin Medical University Cancer Hospital were washed three times with PBS supplemented with 1 $\times$  penicillin/streptomycin and cut into small pieces. The sectioned samples were incubated with 0.001% DNase I (Sigma, MO, USA), 1 mg/ml collagenase IV (Roche, IN, USA), and 1 $\times$  penicillin/streptomycin in DMEM/F12 medium (Lonza) at 37°C for 3 h with rotation. After incubation, the suspension was passed through a 70  $\mu$ m cell strainer (BD Falcon, CA, USA) and centrifuged at 1,000 rpm for 3 min. The pellet was resuspended in 50  $\mu$ l MBM (DMEM/F12 supplemented with 20 ng/ml of bFGF (Invitrogen, CA, USA), 50 ng/ml human EGF (Invitrogen), N2 (Invitrogen), B27 (Invitrogen), 10  $\mu$ M ROCK inhibitor (Enzo Life Sciences, NY, USA) and 1 $\times$  penicillin/streptomycin (Gibco, USA)). Then, 100  $\mu$ l Matrigel (Corning) was added to the 50  $\mu$ l suspension and seeded in prewarmed (37°C) 96-well culture plates (Corning). After Matrigel polymerization at 37°C for 1 h, 120  $\mu$ l of MBM supplemented with or without 20  $\mu$ M of the PKA inhibitor H89 was added to the well. The medium was changed every 4 days.

### Statistical analysis

The data are shown as the mean  $\pm$  SD. The unpaired two-tailed Student's *t*-test was used to compare two independent experimental groups, Kaplan–Meier methods were used for survival curves, and one-way analysis of variance (ANOVA) was used to compare three or more groups. *P* < 0.05 was considered significant for all tests.

## Data availability

All data in this paper are presented in the main text and supplementary materials. The RNA-seq data of H460 (T/T) and H460 (C/C) cells are available in the Gene Expression Omnibus (GEO) database ([www.ncbi.nlm.nih.gov/geo](http://www.ncbi.nlm.nih.gov/geo)) under accession no. GSE213199 (<http://www.ncbi.nlm.nih.gov/geo/query/acc.cgi?acc=GSE213199>). The RNA-seq data of A549 (T/T) and A549 (C/C) cells have been deposited to the GEO database and assigned the identifier accession no. GSE225330 (<http://www.ncbi.nlm.nih.gov/geo/query/acc.cgi?acc=GSE225330>). The allele-specific 4C data of A549 (T/C) cells are available in the GEO database under accession no. GSE213196 (<http://www.ncbi.nlm.nih.gov/geo/query/acc.cgi?acc=GSE213196>).

The 4C data of A549 (T/T) and A549 (C/C) cells have been deposited to the GEO database and assigned the identifier accession no. GSE225518 (<http://www.ncbi.nlm.nih.gov/geo/query/acc.cgi?acc=GSE225518>). The H3K27ac, H3K4me3, H3K27me3, and H3K9me3 ChIP-seq data of H460 (T/T) and H460 (C/C) are available in the GEO database under accession no. GSE213197 (<http://www.ncbi.nlm.nih.gov/geo/query/acc.cgi?acc=GSE213197>). The H3K27ac and H3K4me3 ChIP-seq data of A549 (T/T) and A549 (C/C) have been deposited to the GEO database and assigned the identifier accession no. GSE225332 (<http://www.ncbi.nlm.nih.gov/geo/query/acc.cgi?acc=GSE225332>). The > 300 Mb file with the microscopy images has been uploaded to BioImage Archive and assigned the identifier accession BioStudies S-BIAD624 (<https://www.ebi.ac.uk/biostudies/studies/S-BIAD624>).

**Expanded View** for this article is available [online](#).

### Acknowledgements

This work was supported by the National Natural Science Foundation of China (grants 81825017, 81773034 to Z.L., 82173320, 81872350 to Z.M.), the Ministry of Science and Technology of China (grant 2018YFC1313002 to Z.L.), the Tianjin Municipal Science and Technology Commission (20JCZDJC00110 to Z.L., 18JCZDJC99100 to Z.M.), and the Haihe Laboratory of Cell Ecosystem Innovation Fund (22HHXBSS00025 to Z.L.).

### Author contributions

**Xinyue Lei:** Data curation; formal analysis; supervision; visualization; writing – original draft; project administration; writing – review and editing. **Xiaoling Tian:** Resources; data curation; formal analysis; validation; investigation; methodology; project administration. **Hao Wang:** Resources; formal analysis; methodology. **Xinran Xu:** Data curation; formal analysis; visualization. **Guoli Li:** Resources; supervision. **Wenxu Liu:** Resources; data curation; software; visualization. **Dan Wang:** Resources; data curation; formal analysis; supervision. **Zenguan Xiao:** Resources; validation. **Mengzhe Zhang:** Resources; data curation. **Mulin Jun Li:** Resources; supervision. **Zhenfa Zhang:** Resources. **Zhenyi Ma:** Supervision; validation; visualization. **Zhe Liu:** Conceptualization; resources; funding acquisition; writing – original draft; project administration; writing – review and editing.

### Disclosure and competing interest statement

The authors declare that they have no conflict of interest.

## References

- Bacher CP, Guggiari M, Brors B, Augui S, Clerc P, Avner P, Eils R, Heard E (2006) Transient colocalization of X-inactivation centres accompanies the initiation of X inactivation. *Nat Cell Biol* 8: 293–299
- Bade BC, Dela Cruz CS (2020) Lung cancer 2020 epidemiology, etiology, and prevention. *Clin Chest Med* 41: 1–24
- Bjarnadottir TK, Fredriksson R, Hoglund PJ, Gloriam DE, Lagerstrom MC, Schioth HB (2004) The human and mouse repertoire of the adhesion family of G-protein-coupled receptors. *Genomics* 84: 23–33
- Bosse Y, Amos CI (2018) A decade of GWAS results in lung cancer. *Cancer Epidemiol Biomarkers* 27: 363–379
- Bradley JD, Paulus R, Komaki R, Masters G, Blumenschein G, Schild S, Bogart J, Hu C, Forster K, Magliocco A et al (2015) Standard-dose versus high-dose conformal radiotherapy with concurrent and consolidation

- carboplatin plus paclitaxel with or without cetuximab for patients with stage IIIA or IIIB non-small-cell lung cancer (RTOG 0617): a randomised, two-by-two factorial phase 3 study. *Lancet Oncol* 16: 187–199
- Bray F, Ferlay J, Soerjomataram I, Siegel RL, Torre LA, Jemal A (2018) Global cancer statistics 2018: GLOBOCAN estimates of incidence and mortality worldwide for 36 cancers in 185 countries. *CA Cancer J Clin* 68: 394–424
- Campos EI, Reinberg D (2009) Histones: annotating chromatin. *Annu Rev Genet* 43: 559–599
- Collisson B, Howell JL (2014) The liking-similarity effect: perceptions of similarity as a function of liking. *J Soc Psychol* 154: 384–400
- Dai JC, Zhu M, Wang YZ, Qin N, Ma HX, He YQ, Zhang RX, Tan W, Fan JY, Wang TP et al (2019) Identification of risk loci and a polygenic risk score for lung cancer: a large-scale prospective cohort study in Chinese populations. *Lancet Respir Med* 7: 881–891
- Dong J, Hu ZB, Wu C, Guo H, Zhou BS, Lv JC, Lu DR, Chen KX, Shi YY, Chu MJ et al (2012) Association analyses identify multiple new lung cancer susceptibility loci and their interactions with smoking in the Chinese population. *Nat Genet* 44: 895–899
- Ferlay J, Soerjomataram I, Dikshit R, Eser S, Mathers C, Rebelo M, Parkin DM, Forman D, Bray F (2015) Cancer incidence and mortality worldwide: sources, methods and major patterns in GLOBOCAN 2012. *Int J Cancer* 136: E359–E386
- Fraser P, Bickmore W (2007) Nuclear organization of the genome and the potential for gene regulation. *Nature* 447: 413–417
- Fredriksson R, Gloriam DEI, Högglund PJ, Lagerström MC, Schiöth HB (2003) There exist at least 30 human G-protein-coupled receptors with long Ser/Thr-rich N-termini. *Biochem Biophys Res Commun* 301: 725–734
- Freedman ML, Monteiro ANA, Gayther SA, Coetzee GA, Risch A, Plass C, Casey G, De Biasi M, Carlson C, Duggan D et al (2011) Principles for the post-GWAS functional characterization of cancer risk loci. *Nat Genet* 43: 513–518
- Frisch SM (2001) Tumor suppression activity of adenovirus E1a protein: anoiiks and the epithelial phenotype. *Adv Cancer Res* 80: 39–49
- Gadgeel SM, Ruckdeschel JC, Patel BB, Wozniak A, Konski A, Valdivieso M, Hackstock D, Chen W, Belzer K, Burger AM et al (2011) Phase II study of Pemetrexed and cisplatin, with chest radiotherapy followed by docetaxel in patients with stage III non-small cell lung cancer. *J Thorac Oncol* 6: 927–933
- Glenn TD, Talbot WS (2013) Analysis of Gpr126 function defines distinct mechanisms controlling the initiation and maturation of myelin. *Development* 140: 3167–3175
- Hamann J, Aust G, Araç D, Engel FB, Formstone C, Fredriksson R, Hall RA, Harty BL, Kirchhoff C, Knapp B et al (2015) International Union of Basic and Clinical Pharmacology. XCIV. Adhesion G protein-coupled receptors. *Pharmacol Rev* 67: 338–367
- Hancock DB, Eijgelsheim M, Wilk JB, Gharib SA, Loehr LR, Marcianti KD, Franceschini N, van Durme YMTA, Chen TH, Barr RG et al (2010) Meta-analyses of genome-wide association studies identify multiple loci associated with pulmonary function. *Nat Genet* 42: 45–52
- Heintzman ND, Stuart RK, Hon G, Fu YT, Ching CW, Hawkins RD, Barrera LO, Van Calcar S, Qu CX, Ching KA et al (2007) Distinct and predictive chromatin signatures of transcriptional promoters and enhancers in the human genome. *Nat Genet* 39: 311–318
- Hindorf LA, Sethupathy P, Junkins HA, Ramos EM, Mehta JP, Collins FS, Manolio TA (2009) Potential etiologic and functional implications of genome-wide association loci for human diseases and traits. *Proc Natl Acad Sci USA* 106: 9362–9367
- Hosseini M, Fattahi Z, Abedini SS, Hu H, Ropers HH, Kalscheuer VM, Najmabadi H, Kahrizi K (2019) GPR126: a novel candidate gene implicated in autosomal recessive intellectual disability. *Am J Med Genet A* 179: 13–19
- Javierre BM, Burren OS, Wilder SP, Kreuzhuber R, Hill SM, Sewitz S, Cairns J, Wingett SW, Varnai C, Thiecke MJ et al (2016) Lineage-specific genome architecture links enhancers and non-coding disease variants to target gene promoters. *Cell* 167: 1369–1384.e19
- Kim M, Mun H, Sung CO, Cho EJ, Jeon HJ, Chun SM, Jung DJ, Shin TH, Jeong GS, Kim DK et al (2019) Patient-derived lung cancer organoids as *in vitro* cancer models for therapeutic screening. *Nat Commun* 10: 3991
- Kou I, Takahashi Y, Johnson TA, Takahashi A, Guo L, Dai J, Qiu XS, Sharma S, Takimoto A, Ogura Y et al (2013) Genetic variants in GPR126 are associated with adolescent idiopathic scoliosis. *Nat Genet* 45: 676–679
- Küffer A, Lakkaraju AK, Mogha A, Petersen SC, Airich K, Doucerain C, Marpakwar R, Bakirci P, Senatore A, Monnard A et al (2016) The prion protein is an agonistic ligand of the G protein-coupled receptor Adgrg6. *Nature* 536: 464–468
- Lin L, Zhao J, Hu J, Huang F, Han J, He Y, Cao X (2016) Comparison of the efficacy and tolerability of gefitinib with pemetrexed maintenance after first-line platinum-based doublet chemotherapy in advanced lung adenocarcinoma: single-center experience. *Onco Targets Ther* 9: 6305–6314
- Lochner A, Moolman JA (2006) The many faces of H89: a review. *Cardiovasc Drug Rev* 24: 261–274
- Mogha A, Benesh AE, Patra C, Engel FB, Schoneberg T, Liebscher I, Monk KR (2013) Gpr126 functions in Schwann cells to control differentiation and myelination via G-protein activation. *J Neurosci* 33: 17976–17985
- Mogha A, Harty BL, Carlin D, Joseph J, Sanchez NE, Suter U, Piao XH, Cavalli V, Monk KR (2016) Gpr126/Adgrg6 has Schwann cell autonomous and nonautonomous functions in peripheral nerve injury and repair. *J Neurosci* 36: 12351–12367
- Monk KR, Naylor SG, Glenn TD, Mercurio S, Perlin JR, Dominguez C, Moens CB, Talbot WS (2009) A G protein-coupled receptor is essential for Schwann cells to initiate myelination. *Science* 325: 1402–1405
- Monk KR, Oshima K, Jors S, Heller S, Talbot WS (2011) Gpr126 is essential for peripheral nerve development and myelination in mammals. *Development* 138: 2673–2680
- Moriguchi T, Haraguchi K, Ueda N, Okada M, Furuya T, Akiyama T (2004) DREG, a developmentally regulated G protein-coupled receptor containing two conserved proteolytic cleavage sites. *Genes Cells* 9: 549–560
- Muller H, Gil J, Drinnenberg IA (2019) The impact of centromeres on spatial genome architecture. *Trends Genet* 35: 565–578
- Nedeljkovic M, Sundberg EJ (2020) Cytokines: from basic mechanisms of cellular control to new therapeutics. In *Cold Spring Harbor perspectives in biology*, Leonard WJ, Schreiber RD (eds), pp 90–95. New York, NY: Cold Spring Harbor Laboratory Press
- Paavola KJ, Sidik H, Zuchero JB, Eckart M, Talbot WS (2014) Type IV collagen is an activating ligand for the adhesion G protein-coupled receptor GPR126. *Sci Signal* 7: ra76
- Pang B, Snyder MP (2020) Systematic identification of silencers in human cells. *Nat Genet* 52: 254–263
- Patarroyo M, Tryggvason K, Virtanen I (2002) Laminin isoforms in tumor invasion, angiogenesis and metastasis. *Semin Cancer Biol* 12: 197–207
- Paz-Ares L, Ross H, O'Brien M, Riviere A, Gatzemeier U, Von Pawel J, Kaukel E, Freitag L, Digel W, Bischoff H et al (2008) Phase III trial comparing paclitaxel polyglumex vs docetaxel in the second-line treatment of non-small-cell lung cancer. *Br J Cancer* 98: 1608–1613
- Petersen SC, Luo R, Liebscher I, Giera S, Jeong SJ, Mogha A, Ghidinelli M, Feltri ML, Schöneberg T, Piao X et al (2015) The adhesion GPCR GPR126 has

- distinct, domain-dependent functions in Schwann cell development mediated by interaction with laminin-211. *Neuron* 85: 755–769
- Pogoda HM, Sternheim N, Lyons DA, Diamond B, Hawkins TA, Woods IG, Bhatt DH, Franzini-Armstrong C, Dominguez C, Arana N et al (2006) A genetic screen identifies genes essential for development of myelinated axons in zebrafish. *Dev Biol* 298: 118–131
- Quinodoz SA, Ollikainen N, Tabak B, Palla A, Schmidt JM, Detmar E, Lai MM, Shishkin AA, Bhat P, Takei Y et al (2018) Higher-order inter-chromosomal Hubs Shape 3D Genome Organization in the Nucleus. *Cell* 174: 744–757.e24
- Ravenscroft G, Nolent F, Rajagopalan S, Meireles AM, Paavola KJ, Gaillard D, Alanio E, Buckland M, Arbuckle S, Krivanek M et al (2015) Mutations of GPR126 are responsible for severe arthrogyposis multiplex Congenita. *Am J Hum Genet* 96: 955–961
- Rea S, Eisenhaber F, O'Carroll D, Strahl BD, Sun ZW, Schmid M, Opravil S, Mechtler K, Ponting CP, Allis CD et al (2000) Regulation of chromatin structure by site-specific histone H3 methyltransferases. *Nature* 406: 593–599
- Remon J, Ahn MJ, Girard N, Johnson M, Kim DW, Lopes G, Pillai RN, Solomon B, Villacampa G, Zhou Q (2019a) Advanced-stage non-small cell lung cancer: advances in thoracic oncology 2018. *J Thorac Oncol* 14: 1134–1155
- Remon J, Menis J, Aspeslagh S, Besse B (2019b) Treatment duration of checkpoint inhibitors for NSCLC. *Lancet Respir Med* 7: 835–837
- Remon J, Reguart N, Auclin E, Besse B (2019c) Immune-related adverse events and outcomes in patients with advanced non-small cell lung cancer: a predictive marker of efficacy? *J Thorac Oncol* 14: 963–967
- Senan S, Brade A, Wang LH, Vansteenkiste J, Dakhil S, Biesma B, Aguillo MM, Aerts J, Govindan R, Rubio-Viqueira B et al (2016) PROCLAIM: randomized phase III trial of Pemetrexed-cisplatin or etoposide-cisplatin plus thoracic radiation therapy followed by consolidation chemotherapy in locally advanced nonsquamous non-small-cell lung cancer. *J Clin Oncol* 34: 953–962
- Shaffer JR, Li JX, Lee MK, Roosenboom J, Orlova E, Adhikari K, Gallo C, Poletti G, Schuler-Faccini L, Bortolini MC et al (2017) Multiethnic GWAS reveals polygenic architecture of earlobe attachment. *Am J Hum Genet* 101: 913–924
- Siegel RL, Miller KD, Jemal A (2017) Cancer statistics, 2017. *CA Cancer J Clin* 67: 7–30
- Splinter E, de Laat W (2011) The complex transcription regulatory landscape of our genome: control in three dimensions. *EMBO J* 30: 4345–4355
- Stehlik C, Kroismayr R, Dorfleutner A, Binder BR, Lipp J (2004) VIGR - a novel inducible adhesion family G-protein coupled receptor in endothelial cells. *FEBS Lett* 569: 149–155
- Vansteenkiste J, Crino L, Doooms C, Douillard JY, Faivre-Finn C, Lim E, Rocco G, Senan S, Van Schil P, Veronesi G et al (2014) 2nd ESMO consensus conference on lung cancer: early-stage non-small-cell lung cancer consensus on diagnosis, treatment and follow-up. *Ann Oncol* 25: 1462–1474
- Xia W, Xu J, Yu G, Yao G, Xu K, Ma X, Zhang N, Liu B, Li T, Lin Z et al (2019) Resetting histone modifications during human parental-to-zygotic transition. *Science* 365: 353–360
- Xu N, Tsai CL, Lee JT (2006) Transient homologous chromosome pairing marks the onset of X inactivation. *Science* 311: 1149–1152
- Zappa C, Mousa SA (2016) Non-small cell lung cancer: current treatment and future advances. *Transl Lung Cancer Res* 5: 288–300
- Zheng H, Xie W (2019) The role of 3D genome organization in development and cell differentiation. *Nat Rev Mol Cell Biol* 20: 535–550